Safe and Efficient Model-free Adaptive Control via Bayesian Optimization

Christopher König[1,*], Matteo Turchetta[2,*], John Lygeros[3], Alisa Rupenyan[1,3], Andreas Krause[2]

arXiv:2101.07825v1 [eess.SY] 19 Jan 2021

***Abstract*— Adaptive control approaches yield high-performance controllers when a precise system model or suitable parametrizations of the controller are available. Existing data-driven approaches for adaptive control mostly augment standard model-based methods with additional information about uncertainties in the dynamics or about disturbances. In this work, we propose a purely data-driven, model-free approach for adaptive control. Tuning low-level controllers based solely on system data raises concerns on the underlying algorithm safety and computational performance. Thus, our approach builds on GoOSE, an algorithm for safe and sample-efficient Bayesian optimization. We introduce several computational and algorithmic modifications in GoOSE that enable its practical use on a rotational motion system. We numerically demonstrate for several types of disturbances that our approach is sample efficient, outperforms constrained Bayesian optimization in terms of safety, and achieves the performance optima computed by grid evaluation. We further demonstrate the proposed adaptive control approach experimentally on a rotational motion system.**

I. Introduction

Adaptive control approaches are a desirable alternative to robust controllers in high-performance applications that deal with disturbances and uncertainties in the plant dynamics. Learning uncertainties in the dynamics and adapting have been explored with classical control mechanisms such as Model Reference Adaptive Control (MRAC) [1], [2]. Gaussian processes (GP) have been also used to model the output of a nonlinear system in a dual controller [3], while coupling the states and inputs of the system in the covariance function of the GP model. Learning the dynamics in an $\mathcal{L}_1$-adaptive control approach has been demonstrated in [4], [5].

Instead of modeling or learning the dynamics, the system can be represented by its performance, directly measured from data. Then, the low-level controller parameters can be optimized to fulfill the desired performance criteria. This has been demonstrated for motion systems in [6]–[10]. Such model-free approaches, however, have not been brought to continuous adaptive control, largely because of difficulties in continuously maintaining stability and safety in the presence of disturbances and system uncertainties, and because of the associated computational complexity. Recently, a sample-efficient extension for safe exploration in Bayesian optimization has been proposed [11]. In this paper, we further optimize this algorithm to develop a model-free adaptive control method for motion systems.

Contribution. In this work, we make the following contributions: (1) we extend the GoOSE algorithm for policy search to adaptive control problems; that is, to problems where constant tuning is required due to changes in environmental conditions. (2) We reduce GoOSE's complexity so that it can be effectively used for policy optimization beyond simulations. (3) We show the effectiveness of our approach in extensive evaluations on a real and simulated rotational axis drive, a crucial component in many industrial machines.

A table of symbols can be found in Section IX.

II. Related work

Bayesian optimization. Bayesian optimization (BO) [12] denotes a class of sample-efficient, black-box optimization algorithms that have been used to address a wide range of problems, see [13] for a review. In particular, BO has been successful in learning high-performance controllers for a variety of systems. For instance, [14] learns the parameters of a discrete event controller for a bipedal robot with BO, while [15], trades off real-world and simulated control experiments via BO. In [16], variational autoencoders are combined with BO to learn to control an hexapod, while [17] uses multi-objective BO to learn robust controllers for a pendulum.

Safety-aware BO. Optimization under unknown constraints naturally models the problem of learning in safety-critical conditions, where *a priori* unknown safety constraints must not be violated. In [18] and [19] safety-aware variants of standard BO algorithms are presented. In [20]–[22], BO is used as a subroutine to solve the unconstrained optimization of the augmented Lagrangian of the original problem. While these methods return feasible solutions, they may perform unsafe evaluations. In contrast, the SafeOPT algorithm [23] guarantees safety at all times. It has been used to safely tune a quadrotor controller for position tracking [6], [24]. In [7], it has been integrated with particle swarm optimization (PSO) to learn high-dimensional controllers. Unfortunately, SafeOPT may not be sample-efficient due to its exploration strategy. To address this, many solutions have been proposed. For example, [25] does not actively expand the safe set, which may compromise the optimality of the algorithm but works well for the application considered. Alternatively, StageOPT [26] first expands the safe set and, subsequently, optimizes over it. Unfortunately, it cannot provide good solutions if stopped prematurely. GoOSE [11] addresses this problem by using a separate optimization oracle and expanding the safe set in a goal-oriented fashion only when necessary to evaluate the inputs suggested by the oracle.

This project has been finded by the Swiss Innovation Agency (Innosuisse), grant Nr. 46716, and by the Swiss National Science Foundation under NCCR Automation.

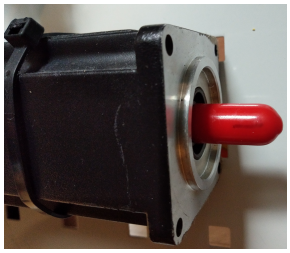
[1] Inspire AG, Zurich, Switzerland
[2] Learning & Adaptive Systems group, ETH Zurich, Switzerland
[3] Automatic Control Laboratory, ETH Zurich, Switzerland
[*] The authors contributed equally.

III. System and problem statement

In this section, we present the system of interest, its control scheme, and the mathematical model we use for our numerical evaluations. Finally, we introduce the safety-critical adaptive control problem we aim to solve.

A. System and controller

The system of interest is a rotational axis drive, a positioning mechanism driven by a synchronous 3 phase permanent magnet AC motor equipped with encoders for position and speed tracking (see Fig. 1). Such systems are routinely used



Param.	Value	Unit
m	0.0191	kgm^2
b	30.08	$\mathrm{kgm}^2/\mathrm{s}$
c_1	$1.78e-3$	Nm
c_2	0.0295	Nm/rad
c_3	0.372	rad
c_4	$8.99e-3$	Nm
c_5	0.11	rad

Fig. 1: Rotational axis drive (left) and its parameters (right).

as components in the semiconductor industry, in biomedical engineering, and in photonics and solar technologies.

We model the system as a combination of linear and nonlinear blocks, where the linear block is modeled as a damped single mass system, following [9]:

$$G(s) := [G_{\mathrm{p}}(s), G_{\mathrm{v}}(s)]^\top = \left[\frac{1}{ms^2+bs}, \frac{1}{ms+b}\right]^\top, \quad (1)$$

where $G_{\mathrm{p}}(s)$ and $G_{\mathrm{v}}(s)$ are the transfer functions respectively from torque to angular position and torque to angular velocity, m is the moment of inertia, and b is the rotational damping coefficient due to the friction. The values of m and b are obtained via least squares fitting and shown in Fig. 1.

Next, we introduce the model for the nonlinear part of the dynamics f_{c}, which we subtract from the total torque signal, see Fig. 2. The nonlinear cogging effects due to interactions between the permanent magnets of the rotor and the stator slots [27] are modelled using a Fourier truncated expansion as $f_{\mathrm{c}}(p) = c_1 + c_2 p + \sum_{k=1}^{n} c_{2k+2} \sin\left(\frac{2k\pi}{c_3} p + c_{2k+3}\right)$ where p is the position, c_1 is the average thrust torque, c_2 is the gradient of the curve, c_3 is the largest dominant period described by the angular distance of a pair of magnets, n is the number of modelled frequencies, and, c_{2k+2} and c_{2k+3} are respectively the amplitudes and the phase shifts of the sinusoidal functions, for $k = 1, 2, \ldots, n$. The parameters $\mathrm{c} := [c_1, \ldots, c_{2n+3}]$ are estimated using least squares error minimization between the modelled cogging torque signals and the measured torque signal at constant velocity to cancel the effects from linear dynamics. The estimates of the parameters are shown in Fig. 1. To model the noise of the system, zero mean white noise with 6.09e-3 Nm variance is added to the torque input signal of the plant.

The system is controlled by a three-level cascade controller shown in Figure 2. The outermost loop controls the position with a P-controller $C_{\mathrm{p}}(s) = K_{\mathrm{p}}$, and the middle loop controls the velocity with a PI-controller $C_{\mathrm{v}}(s) = K_{\mathrm{v}}(1 + \frac{1}{T_{\mathrm{i}} s})$. The innermost loop controls the current of the rotational drive. It is well-tuned and treated as a part of the plant $G(s)$. Feedforward structures are used to accelerate the response of the system. Their gains are well-tuned and not modified during the re-tuning procedure. However, in our experiments, we perturb them to demonstrate that our method can adapt to new operating conditions by adjusting the tunable parameters of the controller.

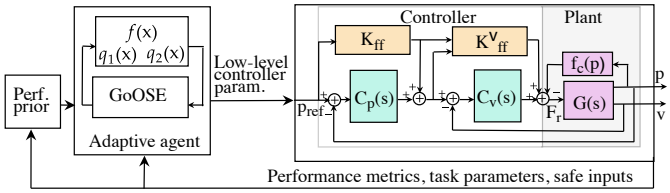


Fig. 2: Scheme of the proposed BO-based adaptive control.

B. Adaptive control approach

In this section, we present the adaptive control problem we aim to solve. In particular, our goal is to tune the parameters of the cascade controller introduced in Section III-A to maximize the tracking accuracy of the system, following [9]. Let $\mathcal{X}$ denote the space of admissible controller parameters, $x = [K_{\mathrm{p}}, K_{\mathrm{v}}, T_{\mathrm{i}}]$, and let $f : \mathcal{X} \to \mathbb{R}$ be the objective measuring the corresponding tracking accuracy. In particular, we define f as the position tracking error averaged over the trajectory induced by the controller $f(x) = \frac{1}{N}\sum_{i=1}^{N} |p_i^{\mathrm{err}}(x)|$, where p_i^{err} is the deviation from the reference position at sampling time i. Crucially, f does not admit a closed-form expression even when the system dynamics are known. However, for a given controller $x \in \mathcal{X}$, the corresponding tracking accuracy $f(x)$ can be obtained experimentally. Notice that f can be extended to include many performance metrics, to minimise oscillations, or to reduce settling time, as in [8], [9].

In practice, we cannot experiment with arbitrary controllers while optimizing f due to safety and performance concerns. Thus, we introduce two constraints that must be satisfied at all times. The first one is a safety constraint $q_1(x)$ defined as the maximum of the fast Fourier transform (FFT) of the torque measurement in a fixed frequency window. The second one is a tracking performance constraint $q_2(x) = |p^{\mathrm{err}}(x)|_\infty$ defined as the infinity norm of the position tracking error. Finally, in reality, the system may be subject to sudden or slow disturbances such as a change of load or a drift in the dynamics due to components wear. Therefore, our goal is to automatically tune the controller parameters of our system to maximize tracking accuracy for varying operating conditions that we cannot control, while never violating safety and quality constraints along the way.

IV. Background

Gaussian processes. A Gaussian process (GP) [28] is a distribution over the space of functions commonly used in non-parametric Bayesian regression. It is fully described by a mean function $\mu : \mathcal{X} \to \mathbb{R}$, which, w.l.o.g, we set to zero for all inputs $\mu(x) = 0, \ \forall x \in \mathcal{X}$, and a kernel function

$k : \mathcal{X} \times \mathcal{X} \to \mathbb{R}$. Given the data set $\mathcal{D} = \{(x_i, y_i\}_{i=1}^t$, where $y_i = f(x_i) + \varepsilon_i$ and $\varepsilon_i \sim \mathcal{N}(0, \sigma^2)$ is zero-mean i.i.d. Gaussian noise, the posterior belief over the function f has the following mean, variance and covariance:

$$\mu_t(x) = \mathbf{k}_t^\top(x)(\mathbf{K}_t + \sigma^2\mathbf{I})^{-1}\mathbf{y}_t, \tag{2}$$

$$k_t(x, x') = k(x, x') - \mathbf{k}_t^\top(x)(\mathbf{K}_t + \sigma^2\mathbf{I})^{-1}\mathbf{k}_t(x'), \tag{3}$$

$$\sigma_t(x) = k_t(x, x), \tag{4}$$

where $\mathbf{k}_t(x) = (k(x_1, x), \ldots, k(x_t, x))$, $\mathbf{K}_t$ is the positive definite kernel matrix $[k(x, x')]_{x,x' \in \mathcal{D}_t}$, and $\mathbf{I} \in \mathbb{R}^{t \times t}$ denotes the identity matrix. In the following, the superscripts f and q denote GPs on the objective and on the constraints.

Multi-task BO. In multi-task BO, the objective depends on the extended input $(x, \tau) \in \mathcal{X} \times \mathcal{T}$, where x is the variable we optimize over and τ is a task parameter set by the environment that influences the objective. To cope with this new dimension, multi-task BO adopts kernels of the form $k_{\text{multi}}((x, \tau), (x', \tau')) = k_\tau(\tau, \tau') \otimes k(x, x')$, where $\otimes$ denotes the Kronecker product. This kernel decouples the correlations in objective values along the input dimensions, captured by k, from those across tasks, captured by k_τ [29].

GoOSE. GoOSE extends any standard BO algorithm to provide high-probability safety guarantees in presence of *a priori* unknown safety constraints. It builds a Bayesian model of the constraints from noisy evaluations based on GP regression. It uses this model to build estimates of two sets: the *pessimistic* safe set, which contains inputs that are safe, i.e., satisfy the constraints, with high probability and the *optimistic* safe set that contains inputs that could potentially be safe. At each round, GoOSE communicates the optimistic safe set to the BO algorithm, which returns the input it would evaluate within this set, denoted as x^*. If x^* is also in the pessimistic safe set, GoOSE evaluates the corresponding objective. Otherwise, it evaluates the constraints at a sequence of provably safe inputs, whose choice is based on a heuristic priority function, that allow us to conclude that x^* either satisfies or violates the constraints with high probability. In the first case, the corresponding objective value is observed. In the second case, x^* is removed from the optimistic safe set and the BO algorithm is queried for a new suggestion. Compared to [23], [26] GoOSE achieves a higher sample efficiency [11] while compared to [18]–[22], it guarantees safety at all times with high probability, under regularity assumptions.

GoOSE assumptions. To infer constraint and objective values of inputs before evaluating them, GoOSE assumes these functions belong to a class of well-behaved functions, i.e., functions with a bounded norm in some reproducing kernel Hilbert space (RKHS) [30]. Based on this assumption, we can build well-calibrated confidence intervals over them. Here, we present these intervals for the safety constraint, q (the construction for f is analogous). Let $\mu_t^q(x)$ and $\sigma_t^q(x)$ denote the posterior mean and standard deviation of our belief over $q(x)$ computed according to Eqs. (2) and (3). We recursively define these monotonically increasing/decreasing lower/upper bounds for $q(x)$: $l_t^q(x) = \max(l_{t-1}^q(x), \mu_{t-1}^q(x) - \beta_{t-1}^q \sigma_{t-1}^q(x))$ and $u_t^q(x) = \min(u_{t-1}^q(x), \mu_{t-1}^q(x) + \beta_{t-1}^q \sigma_{t-1}^q(x))$. The authors of [31], [32] show that, for functions with bounded RKHS norm, an appropriate choice of β_t^q implies that $l_t^q(x) \leq q(x) \leq u_t^q(x)$ for all $t \in \mathbb{R}^+$ and $x \in \mathcal{X}$. However, in practice, a constant value of 3 is sufficient to achieve safety [6], [11], [24].

To start collecting data safely, GoOSE requires knowledge of a set of inputs that are known *a priori* to be safe, denoted as S_0. In our problem, it is easy to identify such set by designing conservative controllers for simplistic first principle models of the system under control.

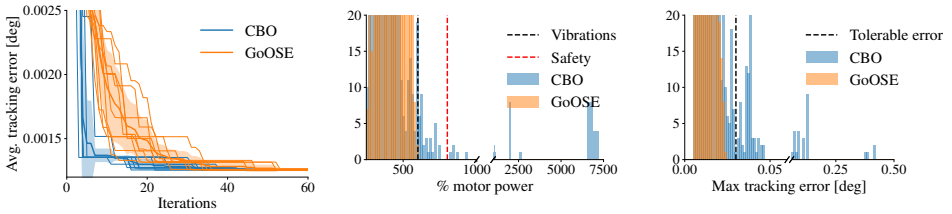
V. GoOSE for adaptive control

In adaptive control, quickly finding a safe, locally optimal controller in response to modified external conditions is crucial. In its original formulation, GoOSE is not suitable to this problem for several reasons: (*i*) it assumes knowledge of the Lipschitz constant of the constraint, which is unknown in practice, (*ii*) it relies on a fine discretization of the domain, which is prohibitive in large domains, (*iii*) it explicitly computes the optimistic safe set, which is expensive, (*iv*) it does not account for external changes it cannot control. In this section, we address these problems step by step and we present the resulting algorithm.

Algorithm 1: GoOSE for adaptive control

Input: Safe seed S_0, $f \sim \mathcal{GP}(\mu^f, k^f; \theta^f)$, $q \sim \mathcal{GP}(\mu^q, k^q; \theta^q)$, $\tau = \tau_0$;
Grid resolution: Δx s.t. $k^q(x, x + \Delta x)(\sigma_\eta^q)^{-2} = 0.95$
while *machine is running* **do**
  $S_t \leftarrow \{x \in \mathcal{X} : u_t^q(x, \tau) \leq \kappa\}$;
  $L_t \leftarrow \{x \in S_t : \exists z \notin S_t$, with $d(x, z) \leq \Delta x\}$;
  $W_t \leftarrow \{x \in L_t : u_t^q(x, \tau) - l_t^q(x, \tau) \geq \epsilon\}$;
  $x^* \leftarrow \texttt{PSO}(S_t, W_t)$;
  if $|f(x^\dagger(\tau)) - l_t^f(x^*, \tau)| \geq \epsilon_{tol}$ **then**
    if $u_t^q(x^*, \tau) \leq \kappa$ **then** evaluate $f(x^*), q(x^*)$, update τ;
    else
      while $\exists x \in W_t$, *s.t.* $g_\epsilon^t(x, x^*) > 0$ **do**
        $x_w^* \leftarrow \arg\min_{x \in W_t} d(x^*, x)$ s.t. $g_\epsilon^t(x, x^*) \neq 0$;
        Evaluate $f(x_w^*), q(x_w^*)$, update τ, S_t, L_t, W_t;
  else
    set system to $x^\dagger(\tau)$, update τ

Task parameter. In general, the dynamics of a controlled system may vary due to external changes. For example, our rotational axis drive may be subject to different loads or the system components may wear due to extended use. As dynamics change, so do the optimal controllers. In this case, we must adapt to new regimes imposed by the environment. To this end, we extend GoOSE to the multi-task setting presented in Section IV by introducing a task parameter τ that captures the exogenous conditions that influence the system's dynamics, and by using the kernel introduced in Section IV. To guarantee safety, we assume that the initial safe seed S_0 contains at least one safe controller for each possible task.



	GoOSE	CBO
It. to conv.	35.5	18
$f(x^\dagger_{\text{grid}})$	1.25	1.25
$(K_\text{p}^\dagger, K_\text{v}^\dagger, T_\text{i}^\dagger)$	$(50, 0.10, 1)$	$(50, 0.09, 1)$
# Violations	0	5
Max. violation	(-,-)	$(6587, 0.128)$

Fig. 3: Comparison of GoOSE and CBO for 10 runs of the stationary control problem. On the left, we see the cost for each run and its mean and standard deviation. The center and right figures show the constraint values sampled by each method. GoOSE reaches the same solution as CBO (table), albeit more slowly (left). However, CBO heavily violates the constraints (center-right).

Algorithm 2: PSO

1 **Input**: Safe set S_t, Boundary W_t, # particles m;
2 $p_i \sim \mathcal{U}(S_t),\ v_i \sim \pm\Delta x,\ i = 1, \cdots, m$;
3 **for** $j \leftarrow 0$ **to** J **do**
4 **for** $i \leftarrow 0$ **to** m **do**
5 $cond \leftarrow u_t^q(p_i^j, \tau) \leq \kappa \vee \exists x \in W_t : g_\epsilon^t(x, p_i^j) > 0$;
6 $cond \leftarrow cond \wedge l_t^f(p_i^j, \tau) < z_i^{j-1}$;
7 **if** $cond$ **then** $z_i^j \leftarrow l_t^f(p_i^j, \tau)$ **else** $z_i^j \leftarrow z_i^{j-1}$;
8 $\overline{z}^j \leftarrow \arg\min_{i=1,\ldots,m} z_i^j$;
9 $r_{1,2} \sim \mathcal{U}([0, 2])$;
10 $v_i^{j+1} \leftarrow \alpha^j v_i^j + r_1(z_i^j - p_i^j) + r_2(\overline{z}^j - p_i^j),\ \forall i$;
11 $\tilde{p}_i^{j+1} \leftarrow p_i^j + v_i^j,\ \forall i$;
12 **return** $\overline{z}^J$

Lipschitz constant. GoOSE uses the Lipschitz constant of the safety constraint L_q, which is not known in practice, to compute the pessimistic safe set and an optimistic upper bound on constraint values. For the pessimistic safe set, we adopt the solution suggested in [6] and use the upper bound of the confidence interval to compute it (see L. 3 of Algorithm 1). While pessimism is crucial for safety, optimism is necessary for exploration. To this end, GoOSE computes an optimistic upper bound for the constraint value at input z based on the lower bound of the confidence interval at another input x as $l_t^q(x, \tau) + L_q d(x, z)$, where $d(\cdot, \cdot)$ is the metric that defines the Lipschitz continuity of q. Here, we approximate this bound with $l_t^q(x, \tau) + \|\mu_t^\nabla(x, \tau)\|_\infty d(x, z)$, where $\mu_t^\nabla(x, \tau)$ is the mean of the posterior belief over the gradient of the constraint induced by our belief over the constraint which, due to properties of GPs, is also a GP. This is a local version of the approximation proposed in [33]. Based on this approximation, we want to determine whether, for the current task τ, an optimistic observation of the constraint at controller x, $l_t^q(x, \tau)$ would allow us to classify as safe a controller z despite an ϵ uncertainty due to noisy observations of the constraint. To this end, we introduce the optimistic, noisy expansion operator

$$g_\epsilon^t(x, z) = \mathbb{I}\left[l_t^q(x, \tau) + \|\mu_t^\nabla(x, \tau)\|_\infty d(x, z) + \epsilon \leq \kappa, \right],$$

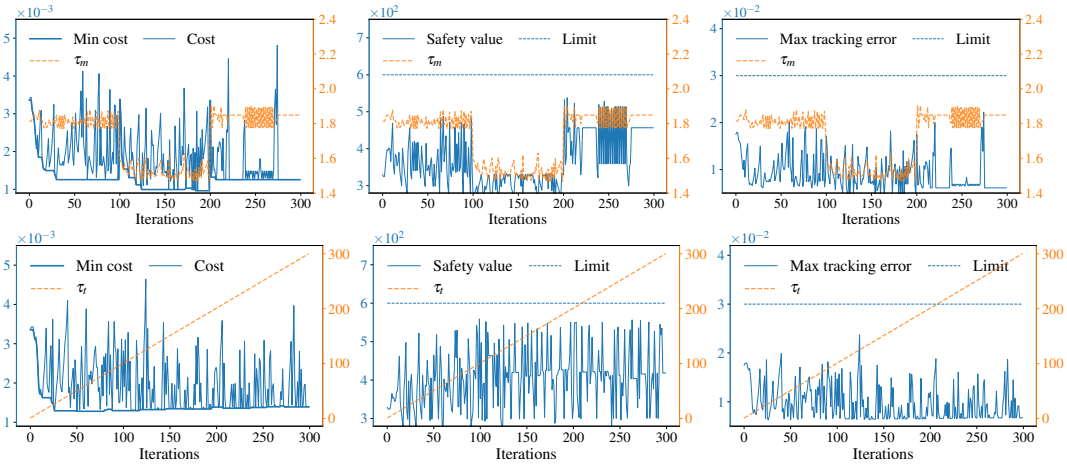
where $\mathbb{I}$ is the indicator function and κ is the upper limit of the constraint. For a safe x, $g_\epsilon^t(x, z) > 0$ determines that: (*i*) z can plausibly be safe and (*ii*) evaluating the constraint at x could include z in the safe set.

Optimization and optimistic safe set. Normally, GoOSE explicitly computes the optimistic safe set and uses GP-LCB [32] to determine the next input where to evaluate the objective, x^*. In other words, GoOSE solves $x_t^* = \arg\min_{x \in S_t^o} \mu_{t-1}^f(x) - \beta_{t-1}^f \sigma_{t-1}^f(x)$, where S_t^o is the optimistic safe set at iteration t. However, this requires a fine discretization of the domain $\mathcal{X}$ to represent S_t^o as finite set of points in $\mathcal{X}$, which does not scale to large domains. Moreover, the recursive computation of S_t^o is expensive and not well suited to the fast responses required by adaptive control. Similarly to [7], here we rely on particle swarm optimization (PSO) [34] to solve this optimization problem, which checks that the particles belong to the one-step optimistic safe set as the optimization progresses and avoids computing it explicitly. We initialize m particles positioned uniformly at random within the discretized pessimistic safe set with grid resolution Δx, velocity Δx with random sign (L. 2 of Algorithm 2) and fitness equal to the lower bound of the objective $l_t^f(\cdot)$. If a particle belongs to the optimistic safe set (L. 5) and its fitness improves (L. 6), we update its best position. This step lets the particle diffuse into the optimistic safe set without computing it explicitly. Subsequently, we update the particles' positions (L. 11) and velocities (L. 10) based on the particles' best position z_i^j and overall best position $\overline{z}^j$, which is updated in L. 8.

Algorithm. We are ready to present our variant of GoOSE for adaptive control. We start by computing the pessimistic safe set S_t (L. 3 of Algorithm 1) on a grid with lengthscale-dependent resolution Δx, its boundary L_t (L. 4) and the uncertain points on its boundary W_t (L. 5), which are used to determine whether controllers belong to the optimistic safe set. Based on these, a new suggestion x^* is computed (L. 6). If its lower bound is close to the best observation for the current task $x^\dagger(\tau) = \arg\min_{\{(x', \tau', f(x')) \in \mathcal{D} : \tau' = \tau\}} f(x')$, we stop (L. 7). Otherwise, if the suggestion is safe, we evaluate it and possibly update the task parameter (L. 8). Finally, if we are not sure it is safe, we evaluate all the expanders x_w^* in increasing order of distance from the suggestion x^*, until either x^* is in the pessimistic safe set and can be evaluated or there are no expanders for x^* and a new query to PSO is made (L. 11 and 12). During this inner loop the task parameter is constantly updated.

VI. Numerical Results

We first apply Algorithm 1 to tune the controller in Fig. 2, simulating the system model in Section III in stationary conditions. Later, we use our method for adaptive control of instantaneous and slow-varying changes of the plant. In



Task (τ_m)	1.81	1.52	1.84
It. to conv.	100	95	65
$f(x^\dagger_\mathrm{grid}(\tau_\mathrm{m}))$	1.27	0.97	1.27
$f(x^\dagger(\tau_\mathrm{m}))$	1.26	0.98	1.26
$K_\mathrm{p}^\dagger$	50	49	50
$K_\mathrm{v}^\dagger$	0.10	0.11	0.10
$T_\mathrm{i}^\dagger$	1	1	1

Task (τ_t)	30	300
$f(x^\dagger_\mathrm{grid}(\tau_\mathrm{t}))$	1.28	1.41
$f(x^\dagger(\tau_\mathrm{t}))$	1.3	1.39
$K_\mathrm{p}^\dagger$	46	50
$K_\mathrm{v}^\dagger$	0.09	0.08
$T_\mathrm{i}^\dagger$	1	1

(a) Minimum and observed cost f (b) Safety constraint q_1. (c) Tracking error constraint q_2.

Fig. 4: Cost (left), safety constraint (center) and performance constraint (right) for the simulated adaptive control experiments with sudden change of the moment of inertia m (upper) and a slow change of the rotational damping b (lower). The thins lines show the values for each experiment. The thick one shows the best cost found for the current task. The tables show the mean values over 10 repetitions for these experiments. GoOSE quickly finds optimal solutions and is able to adapt to both kind of disturbances.

Section IX, we present an ablation study that investigates the impact of the task parameter on these problems.

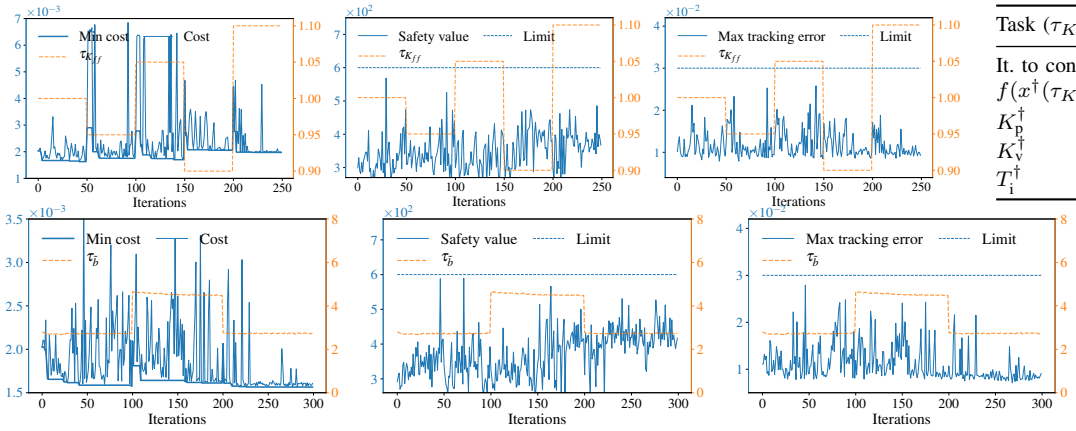
The optimization ranges of the controller parameters are set to $K_\mathrm{p} \in [5, 50]$, $K_\mathrm{v} \in [0.1, 0.11]$ for the position and velocity gains, and $T_\mathrm{i} \in [1, 10]$ for the time constant. For each task, GoOSE returns the controller corresponding to the best observation, $x^\dagger(\tau) = (K_\mathrm{p}^\dagger, K_\mathrm{v}^\dagger, T_\mathrm{i}^\dagger)$. The cost $f(\mathrm{x})$ is provided in $[\deg 10^{-3}]$ units. We denote the 'true' optimal controller computed via grid search as $x^\dagger_\mathrm{grid}$. Due to noise, not even this controller can achieve zero tracking error, see the table in Fig. 3. We use a zero mean prior and squared exponential kernel with automatic relevance determination, with length scales for each dimension $[l_{K_\mathrm{p}}, l_{K_\mathrm{v}}, l_{T_\mathrm{i}}, l_\mathrm{m}, l_{K_\mathrm{ff}}, l_{\tilde{b}}] = [30, 0.03, 3, 0.5, 0.3, 5]$, identical for f, q_1 and q_2 for the numerical simulations and the experiments on the system. The likelihood variance is adjusted separately for each GP model.

Control for stationary conditions. In this section, we compare GoOSE to CBO for controller tuning [10] in terms of the cost and the safety and performance constraints introduced in Section III when tuning the plant under stationary conditions. We benchmark these methods against exhaustive grid-based evaluation using a grid with $5 \times 11 \times 10$ points.

For each algorithm, we run 10 independent experiments, which vary due to noise injected in the simulation. Each experiment starts from the safe controller $[K_\mathrm{p}, K_\mathrm{v}, T_\mathrm{i}] = [15, 0.05, 3]$. The table in Fig. 3 shows the median number of iterations needed to minimize the cost. Fig. 3 (left) shows the convergence of both algorithms for each repetition. While both algorithms converge to the optimum, GoOSE prevents constraint violations for all iterations (see Fig. 3). In contrast, CBO violates the constraints in 27.8% of the iterations to convergence, reaching far in the unsafe range beyond the safety limit of acceptable vibrations in the system (Fig. 3, center), showing that additional safety-related measures are required. While the constraint violations incurred by CBO can be limited in stationary conditions by restricting the optimization range, this is not possible for adaptive control.

Adaptive control for instantaneous changes. We show how our method adapts to instantaneous change in the load of the system. We modify the moment of inertia m and estimate this from the system data. We inform the algorithm of the operating conditions through a task parameter, $\tau_\mathrm{m} = \log 10(\frac{1}{N}\sum_1^N |\mathrm{FFT}(v - v_\mathrm{ff})|)$, which is calculated from the velocity measurement v, using the feed-forward signal v_ff from position to velocity. This data-driven task parameter exploits the differences in the levels of noise in the velocity signal corresponding to different values of the moment of inertia m. As the velocity also depends on the controller parameters, configurations in a range of ± 0.15 of the current τ_m value are treated as the same task configuration. The algorithm is initialized with $[K_\mathrm{p}, K_\mathrm{v}, T_\mathrm{i}] = [15, 0.05, 3]$ as safe seed for all tasks. The moment of inertia of the plant m is switched every 100 iterations. The table in Fig. 4 summarizes 10 repetitions of the experiment with a stopping criterion set to $\epsilon_\mathrm{tol} = 0.002$. Fig. 4 (top left) shows the sampled cost and the task parameters for one run, and the running minimum for each task. We clearly see that GoOSE quickly finds a high performing controller for the initial operating conditions (m = 0.0191kgm^2). Subsequently, it adapts K_p and K_v in few iterations to the new regime (m = 0.0382kgm^2) due to the capability of the GP model to generalize across tasks (Fig. 4, top table). Finally, when the system goes back to the initial regime, GoOSE immediately finds a high-performing controller and manages to marginally improve over it. In particular, the best cost $f(x^\dagger(\tau_\mathrm{m}))$ found for each condition coincides with the optimum obtained by grid evaluation $f(x^\dagger_\mathrm{grid}(\tau_\mathrm{m}))$. Moreover, Fig. 4 (top center left and right) shows that the constraints are never violated.

Adaptive control for gradual changes. We show how our method adapts to slow changes in the dynamics. In particular, we let the rotation damping coefficient increase linearly with time: $b(t) = b_0(1 + \frac{t}{1000})$, where $b_0 = 30.08$kgm^2/s. In this case, time is the task parameter and, therefore, we use the temporal kernel $k(t, t') = (1 - \epsilon_t)^{|t-t'|/2}$ [35] as task kernel



Task ($\tau_{K_{ff}}$)	1.0	0.95	1.05	0.9	1.1
It. to conv.	50	49	47	33	16
$f(x^\dagger(\tau_{K_{ff}}))$	1.63	1.75	1.7	2.07	1.98
$K_\mathrm{p}^\dagger$	37	43	50	50	50
$K_\mathrm{v}^\dagger$	.08	.09	.09	.09	.09
$T_\mathrm{i}^\dagger$	1	10	10	9	8

Task ($\tau_{\tilde{b}}$)	2.72	4.53	2.73
It. to conv.	99	78	19
$f(x^\dagger(\tau_{\tilde{b}}))$	1.59	1.61	1.59
$K_\mathrm{p}^\dagger$	32	30	37
$K_\mathrm{v}^\dagger$	.09	.09	.1
$T_\mathrm{i}^\dagger$	6	7	7

(a) Minimum and observed cost f. (b) Safety constraint q_1. (c) Tracking error constraint q_2.

Fig. 5: Cost (left), safety constraint (center), performance constraint (right) and summary (table) for the real-world adaptive control experiments with sudden change of the feed-forward gain K_ff (upper) and rotational damping $\tilde{b}$ (lower). The thins lines show the values for each experiment. The thick one shows the best cost found for the current task. GoOSE quickly finds optimal controllers for all the regimes (left) without violating the constraints (center-right) despite the location of the optimum keeps changing (table).

with $\epsilon_t = 0.0001$. This kernel increases the uncertainty in already evaluated samples with time. To incorporate the drift of the dynamics, we evaluate the best sample $x^\dagger$ in Algorithm 1 with respect to the stopping criterion threshold $\epsilon_\mathrm{tol} = 0.001$ in a moving window of the last 30 iterations. Learning is slower, due to the increased uncertainty of old data points. On average, the stopping criterion (L. 7 in Algorithm 1) is fulfilled in 74 out of 300 iterations. The optimum increases, (Fig. 4, bottom left and table), corresponding to a change in the controller parameters. In the second half of the experiment the cost decreases, and reaches optimum more often, as the GPs successfully learn the trend of the parameter $b(t)$. There were no constraint violations in any of the repetitions, see Fig. 4 (bottom center left and right).

VII. Experimental Results

We now demonstrate the proposed adaptive control algorithm on a rotational drive system. The system has an encoder resolution of $\Delta p = 1\,\mathrm{deg} \times 10^{-7}$ for the angular position, $\Delta v = 0.0004$ RPM for the angular velocity and $\Delta T = 0.0008$ Nm for the torque. The angular position of the system has no hardware limit. The limits of the angular velocity and the torque are $v_\mathrm{lim} = 50$ RPM and $T_\mathrm{lim} = 3.48$ Nm, respectively. First, we show how the controller parameters adapt when the algorithm is explicitly informed about a change in the feed-forward gain K_ff. We then demonstrate the performance when an external change occurs, corresponding to change in the rotational resistance, which can be estimated from the system's data. The optimization ranges and the kernels hyperparameters are the same as in Section VI. The likelihood variance is adjusted separately for each GP model.

Adaptive control for internal parameter change. We start an experiment with the nominal feed forward gain, $K_\mathrm{ff} = 1$, and switch it subsequently four times between 0.9 and 1.1 in intervals of 50 iterations. For each value of K_ff, the starting point is a safe sample, collected with $[K_\mathrm{p}, K_\mathrm{v}, T_\mathrm{i}] = [15, 0.05, 3]$. The value of K_ff is used as task parameter τ_{K_ff}. The stopping criterion is set to $\epsilon_\mathrm{tol} = 0.001$.

The convergence of the optimization accelerates with increasing data. Fig. 5 (top left) shows that convergence is not reached for the nominal K_ff during the first 50 iterations, whereas the last configuration with $\tau_{K_\mathrm{ff}} = 1.1$ requires only 16 until convergence, showing that learning is efficient, even if the optimum shifts w.r.t. the configuration. Constraint violations are completely prevented for all tasks parameters, as shown in Fig. 5 (top center and right).

Adaptive control for external parameter change. We now validate experimentally the change introduced to the controller by modifying the friction $\tilde{b}$ in the system, which is related to the non-linearity in the dynamics of the plant. We estimate the change in $\tilde{b}$ by the average torque measurement of the system and provide it as task parameter $\tau_{\tilde{b}}$, as shown in Fig. 5 (bottom). We start with optimizing the nominal controller parameters for 100 iterations, followed by an increase of $\tilde{b}$ (and of $\tau_{\tilde{b}}$ accordingly), which is achieved by wrapping elastic bands around the rotational axis and fixing them at the frame of the system. In the last 100 iterations we switch back to the nominal condition. The stopping criterion is set to $\epsilon_\mathrm{tol} = 0.001$. Since $\tau_{\tilde{b}}$ is not fixed and is influenced by noise, all configurations with $\tau_{\tilde{b}}$ in a range of ± 0.1 of the current $\tau_{\tilde{b}}$ value are treated as the same task configuration. The cost increases after the first intervention, then reaches close to nominal values in 10 iterations, and adapts almost instantaneously at the next $\tau_{\tilde{b}}$ switch (Fig. 5, bottom left). The constraints are never violated (Fig. 5, bottom center, right).

VIII. Conclusion

We present a model-free approach to safe adaptive control. To this end, we introduce several modifications to GoOSE, a safe Bayesian optimization method, to enable its practical use on a rotational motion system. We demonstrate numerically and experimentally that our approach is sample efficient, safe, and achieves the optimal performance for different types of disturbances encountered in practice. Our approach can be further extended by including multiple performance metrics in the optimization objective, or gradually tightening the constraints, once sufficient system data is available.

IX. Appendix

Here, we study the impact of tracking the task parameter and adapting to its changes on the performance and safety of the algorithm. To this end, we repeat the numerical experiments for instantaneous and gradual changes presented in Section VI and the experiment for internal parameter changes on the real system presented in Section VII without explicitly modeling the task parameter in our algorithm, and compare the results with those obtained modeling it.

In general, the change in systems dynamics that are induced by a change in external conditions and that are captured by the task parameter greatly impacts the performance and safety of the system when a given controller is applied. As a result, for a given controller x, the algorithm is likely to observe widely different cost and constraints values depending on the task. Without the additional degree of freedom provided by the explicit modelling of the task parameter, the GP model must do its best to make sense out of widely different observations corresponding to the same controller that are too large to be explained by the observation noise. Therefore, we expect this degradation in the quality of the model to induce poor predictive distributions and, therefore, to lead to undesirable and unpredictable behavior of the algorithm.

Numerical results. We start by showing the results obtained for the numerical experiments in Fig. 6. The top panel shows the performance of the algorithm for the instantaneous change of the moment of inertia in the system, and the bottom panel demonstrates the performance during a gradual linear change in the rotational damping. In both cases, the algorithm does not model these changes.

The first experiment replicates exactly the one we presented in the top of Fig. 4. Initially, m is $0.0191\mathrm{kgm}^2$, which induces an average value of τ_m over the duration of the task of 1.83, then doubles to $0.0382\mathrm{kgm}^2$, which induces a lower average value $\tau_m = 1.5$ as the higher moment of inertia reduces the effect of the noise, and switches back to $0.0191\mathrm{kgm}^2$, which, due to the model mismatch, induces an even higher average value of $\tau_m = 2$. Notice that, even though the task parameter τ_m is not provided to the algorithm, we still plot it to show where the tasks switch. During the initial phase of the optimization, the algorithm only experiences one task and, therefore, it is not affected by the fact that it is not modeling the task explicitly. In this phase, an optimum is found after the initial 100 iterations. In the second phase, when m increases, the control task becomes effectively easier. Therefore, the algorithm still manages to control the system and to slightly improve the performance. In this phase, aggressive controllers are classified as safe. This is because they do not induce dangerous vibrations in the system due to the increased moment of inertia. However, switching back to the first, lower value of m creates problems. This is due to two main facts: (*i*) controllers that were previously deemed safe due to the high value of m are not anymore. However, since τ_m is not modelled, the algorithm is not aware of this. (*ii*) the GP is conditioned on highly conflicting observations induced by the different tasks that cannot explain through measurement noise. As a consequence, the confidence intervals it provides deteriorate. This results in multiple violations of both constraints.

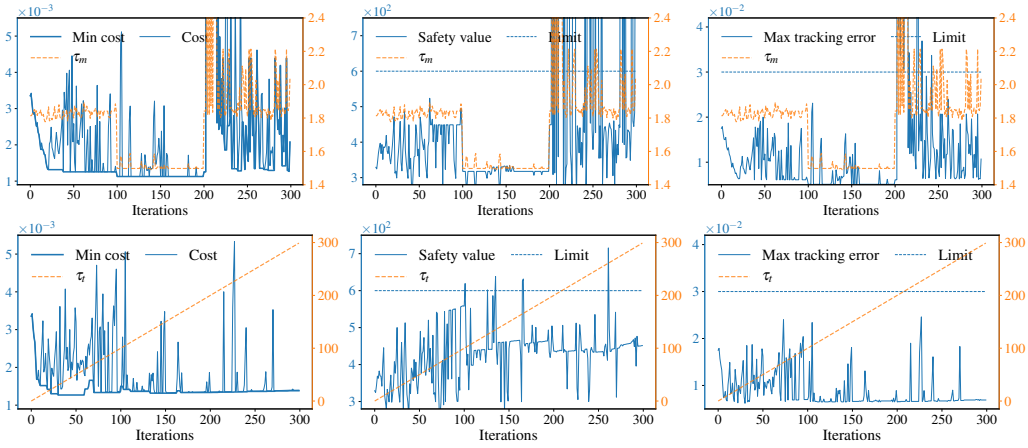
The second numerical experiment replicates the one shown at the bottom of Fig. 4. Although the task parameter is no longer tracked, the 30 iterations window for $x^\dagger$ in Algorithm 1 is kept in the algorithm as an adaptive component. However, this adaptive component alone is not sufficient since the GPs are not able to distinguish between old, less accurate data and new, more accurate data without keeping track of the task parameter. Therefore, as the rotation damping coefficient b increases, the system becomes less robust towards aggressive controllers and the algorithm starts using unsafe parameter settings that used to be safe in previous iterations (see figure Fig. 6 bottom).

Experimental result. In comparison to the two numerical experiments of figure Fig. 6, where we see that the algorithm fails in maintaining safety when we don't inform the GPs about a system relevant change, in this experiment we show that the performance can also deteriorate, without loosing stability. The internal change of K_{ff} has a marginal influence on the set of stable controller parameters. However, the table in Fig. 5 shows that it greatly influences the location of the optimal parameters within this set. Without tracking a task parameter representing the change in K_{ff}, the algorithm optimizes the objective function for the initial value of K_{ff}. Since there is no controller in later stages that outperforms the optimum of the first stage, the algorithm quickly reaches the termination criterion and applies the optimal controller found in the the first stage to the system. This results in suboptimal costs as can be seen by comparing Figs. 5 and 6 (left plots and tables). Furthermore, similar to the experiments of Fig. 6, some parameter settings used by the algorithm after switching the initial K_{ff} value violate the safety or the performance constraint, since similar settings were accepted as safe in prior configurations/tasks.

List of Symbols

The next list describes several symbols that we used throughout the paper and their explanation.

$\mathcal{D}$	Data set
$\mathcal{X}$	Space of admissible controllers
$g_\epsilon^t(x, z)$	Optimistic noisy expansion operator
K_{p}	Position proportional gain
$K_{\mathrm{p}}^\dagger$	Position gain in $x^\dagger$
K_{v}	Velocity proportional gain
$K_{\mathrm{v}}^\dagger$	Velocity gain in $x^\dagger$
μ	GP mean
$\overline{z}_i$	Overall particles best position
x^*	Recommendation of PSO
τ	Task parameter
T_{i}	Velocity time constant
$T_{\mathrm{i}}^\dagger$	Time constant in $x^\dagger$
$x^\dagger(\tau)$	Feasible controller corresponding to best observed cost for task τ

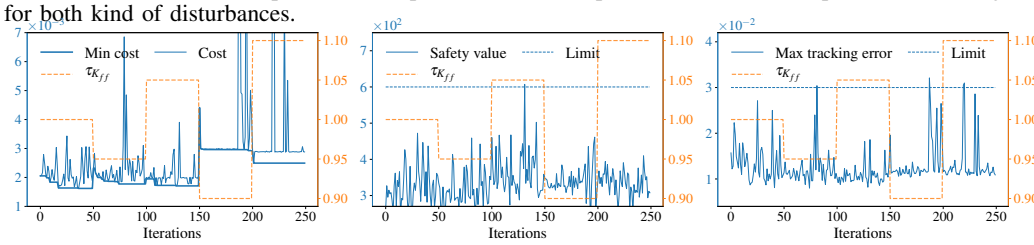


τ_{m}	1.83	1.5	2
$f(x^{\dagger}_{\mathrm{grid}}(\tau_{\mathrm{m}}))$	1.27	0.97	1.27
$f(x^{\dagger}(\tau_{\mathrm{m}}))$	1.26	1.03	1.39
$K^{\dagger}_{\mathrm{p}}$	50	46.73	46.73
$K^{\dagger}_{\mathrm{v}}$	0.095	0.11	0.11
$T^{\dagger}_{\mathrm{i}}$	1	1	1

τ_{t}	30	300
$f(x^{\dagger}_{\mathrm{grid}}(\tau_{\mathrm{t}}))$	1.28	1.41
$f(x^{\dagger}(\tau_{\mathrm{t}}))$	1.30	1.40
$K^{\dagger}_{\mathrm{p}}$	46.7	50
$K^{\dagger}_{\mathrm{v}}$	0.095	0.086
$T^{\dagger}_{\mathrm{i}}$	1	1

(a) Minimum and observed cost f (b) Safety constraint q_1. (c) Tracking error constraint q_2.

Fig. 6: Cost (left), safety constraint (center) and performance constraint (right) for the simulated optimization experiments with sudden change of the moment of inertia m (upper) and a slow change of the rotational damping b (lower) without tracking of the task parameter. The tables summarize the optimization experiments for 10 repetitions. Without task parameter tracking GoOSE results in unsafe behavior for both kind of disturbances.



$\tau_{K_{\mathrm{ff}}}$	1.0	0.95	1.05	0.9	1.1
$f(x^{\dagger})$	1.62	2.08	2.01	3	2.89
$K^{\dagger}_{\mathrm{p}}$	25	25	25	25	25
$K^{\dagger}_{\mathrm{v}}$	.07	.07	.07	.07	.07
$T^{\dagger}_{\mathrm{i}}$	3	3	3	3	3

(a) Minimum and observed cost f. (b) Safety constraint q_1. (c) Tracking error constraint q_2.

Fig. 7: Cost (left), safety constraint (center), performance constraint (right) and summary (table) for the real-world adaptive control experiments with sudden change of the feed-forward gain K_{ff}, without considering the task parameter. The table summarizes the performance of the algorithm on the real system for 10 different experiments. Without keeping track of the task parameter, the cost for each different K_{ff} after the first is higher, compared to task parameter tracking. While safety is mostly maintained, the performance constraint is violated.

$x^{\dagger}_{\mathrm{grid}}(\tau)$	Best feasible controller computed with grid search for task τ
f	Objective (Average tracking error)
k	GP kernel
L	Safe set boundary
L_q	Lipschitz constant
$l_t(x)$	Lower bound of confidence interval
q_1	Safety constraint (FFT of the torque)
q_2	Performance constraint (Max tracing error)
S	Safe set
S^o	Optimistic safe set
S_0	Initial safe seed
$u_t(x)$	Upper bound of confidence interval
W	Uncertain points on safe set boundary
x^*_w	Expander
z_i	i^{th} particle best position

References

[1] G. Chowdhary, H. A. Kingravi, J. P. How, and P. A. Vela, "Bayesian nonparametric adaptive control using Gaussian processes," *IEEE Transactions on Neural Networks and Learning Systems*, vol. 26, no. 3, pp. 537–550, 2015.

[2] R. C. Grande, G. Chowdhary, and J. P. How, "Experimental validation of Bayesian nonparametric adaptive control using Gaussian processes," *Journal of Aerospace Information Systems*, vol. 11, no. 9, pp. 565–578, 2014.

[3] D. Sbarbaro and R. Murray-Smith, *Self-tuning Control of Non-linear Systems Using Gaussian Process Prior Models*. Berlin, Heidelberg: Springer Berlin Heidelberg, 2005, pp. 140–157.

[4] A. Gahlawat, P. Zhao, A. Patterson, N. Hovakimyan, and E. Theodorou, "L1-gp: L1 adaptive control with Bayesian learning," ser. Proceedings of Machine Learning Research, A. M. Bayen, A. Jadbabaie, G. Pappas, P. A. Parrilo, B. Recht, C. Tomlin, and M. Zeilinger, Eds., vol. 120. The Cloud: PMLR, 10–11 Jun 2020, pp. 826–837.

[5] D. D. Fan, J. Nguyen, R. Thakker, N. Alatur, A.-a. Agha-mohammadi, and E. A. Theodorou, "Bayesian Learning-Based Adaptive Control for Safety Critical Systems," *arXiv e-prints*, p. arXiv:1910.02325, Oct. 2019.

[6] F. Berkenkamp, A. P. Schoellig, and A. Krause, "Safe controller optimization for quadrotors with Gaussian processes," *CoRR*, vol. abs/1509.01066, 2015. [Online]. Available: http://arxiv.org/abs/1509.01066

[7] R. R. Duivenvoorden, F. Berkenkamp, N. Carion, A. Krause, and A. P. Schoellig, "Constrained Bayesian optimization with particle swarms for safe adaptive controller tuning," *IFAC-PapersOnLine*, vol. 50, no. 1, pp. 11 800 – 11 807, 2017, 20th IFAC World Congress.

[8] M. Khosravi, V. Behrunani, P. Myszkorowski, R. S. Smith, A. Rupenyan, and J. Lygeros, "Performance-Driven Cascade Controller Tuning with Bayesian Optimization," *arXiv e-prints*, p. arXiv:2007.12536, Jul. 2020.

[9] M. Khosravi, V. Behrunani, R. S. Smith, A. Rupenyan, and J. Lygeros, "Cascade Control: Data-Driven Tuning Approach Based on Bayesian Optimization," *arXiv e-prints*, p. arXiv:2005.03970, May 2020.

[10] C. König, M. Khosravi, M. Maier, R. S. Smith, A. Rupenyan, and J. Lygeros, "Safety-Aware Cascade Controller Tuning Using Constrained Bayesian Optimization," *arXiv e-prints*, p. arXiv:2010.15211, Oct. 2020.

[11] M. Turchetta, F. Berkenkamp, and A. Krause, "Safe exploration for interactive machine learning," in *Advances in Neural Information Processing Systems*, 2019, pp. 2891–2901.

[12] J. Mockus, *Bayesian Approach to Global Optimization: Theory and Applications*, ser. Mathematics and its Applications. Springer Netherlands, 2012.

[13] B. Shahriari, K. Swersky, Z. Wang, R. P. Adams, and N. De Freitas, "Taking the human out of the loop: A review of Bayesian optimization," *Proceedings of the IEEE*, vol. 104, no. 1, pp. 148–175, 2015.

[14] R. Calandra, A. Seyfarth, J. Peters, and M. P. Deisenroth, "Bayesian optimization for learning gaits under uncertainty," *Annals of Mathematics and Artificial Intelligence*, vol. 76, no. 1, pp. 5–23, 2016.

[15] A. Marco, F. Berkenkamp, P. Hennig, A. P. Schoellig, A. Krause, S. Schaal, and S. Trimpe, "Virtual vs. real: Trading off simulations and physical experiments in reinforcement learning with Bayesian optimization," *2017 IEEE International Conference on Robotics and Automation (ICRA)*, pp. 1557–1563, 2017.

[16] R. Antonova, A. Rai, T. Li, and D. Kragic, "Bayesian optimization in variational latent spaces with dynamic compression," in *Conference on Robot Learning*. PMLR, 2020, pp. 456–465.

[17] M. Turchetta, A. Krause, and S. Trimpe, "Robust model-free reinforcement learning with multi-objective Bayesian optimization," *arXiv preprint arXiv:1910.13399*, 2019.

[18] J. Gardner, M. Kusner, Zhixiang, K. Weinberger, and J. Cunningham, "Bayesian optimization with inequality constraints," in *Proceedings of the 31st International Conference on Machine Learning*, ser. Proceedings of Machine Learning Research, E. P. Xing and T. Jebara, Eds., vol. 32, no. 2. Bejing, China: PMLR, 22–24 Jun 2014, pp. 937–945.

[19] J. M. Hernández-Lobato, M. A. Gelbart, M. W. Hoffman, R. Adams, and Z. Ghahramani, "Predictive entropy search for Bayesian optimization with unknown constraints," in *ICML*, 2015.

[20] V. Picheny, R. B. Gramacy, S. Wild, and S. Le Digabel, "Bayesian optimization under mixed constraints with a slack-variable augmented lagrangian," in *Advances in neural information processing systems*, 2016, pp. 1435–1443.

[21] R. B. Gramacy, G. A. Gray, S. Le Digabel, H. K. Lee, P. Ranjan, G. Wells, and S. M. Wild, "Modeling an augmented lagrangian for blackbox constrained optimization," *Technometrics*, vol. 58, no. 1, pp. 1–11, 2016.

[22] S. Ariafar, J. Coll-Font, D. H. Brooks, and J. G. Dy, "Admmbo: Bayesian optimization with unknown constraints using admm." *Journal of Machine Learning Research*, vol. 20, no. 123, pp. 1–26, 2019.

[23] Y. Sui, A. Gotovos, J. W. Burdick, and A. Krause, "Safe exploration for optimization with Gaussian processes," in *International Conference on Machine Learning (ICML)*, 2015.

[24] F. Berkenkamp, A. Krause, and A. P. Schoellig, "Bayesian optimization with safety constraints: Safe and automatic parameter tuning in robotics," *CoRR*, vol. abs/1602.04450, 2016.

[25] M. Fiducioso, S. Curi, B. Schumacher, M. Gwerder, and A. Krause, "Safe contextual Bayesian optimization for sustainable room temperature pid control tuning," *arXiv preprint arXiv:1906.12086*, 2019.

[26] Y. Sui, V. Zhuang, J. W. Burdick, and Y. Yue, "Stagewise safe Bayesian optimization with Gaussian processes," *arXiv preprint arXiv:1806.07555*, 2018.

[27] F. Villegas, R. Hecker, M. Peña, D. Vicente, and G. Flores, "Modeling of a linear motor feed drive including pre-rolling friction and aperiodic cogging and ripple," *The International Journal of Advanced Manufacturing Technology*, vol. 73, 07 2014.

[28] C. E. Rasmussen, "Gaussian processes for machine learning." MIT Press, 2006.

[29] K. Swersky, J. Snoek, and R. Adams, "Multi-task Bayesian optimization," *Advances in Neural Information Processing Systems*, 01 2013.

[30] B. Scholkopf and A. J. Smola, *Learning with kernels: support vector machines, regularization, optimization, and beyond*. Adaptive Computation and Machine Learning series, 2018.

[31] S. R. Chowdhury and A. Gopalan, "On kernelized multi-armed bandits," *arXiv preprint arXiv:1704.00445*, 2017.

[32] N. Srinivas, A. Krause, S. M. Kakade, and M. Seeger, "Gaussian process optimization in the bandit setting: No regret and experimental design," *arXiv preprint arXiv:0912.3995*, 2009.

[33] J. González, Z. Dai, P. Hennig, and N. Lawrence, "Batch Bayesian optimization via local penalization," in *Artificial intelligence and statistics*, 2016, pp. 648–657.

[34] S. Kiranyaz, T. Ince, and M. Gabbouj, *Multidimensional particle swarm optimization for machine learning and pattern recognition*. Springer, 2014.

[35] I. Bogunovic, J. Scarlett, and V. Cevher, "Time-varying Gaussian process bandit optimization," 2016.